Electronic Supplementary Material (ESI) for Physical Chemistry Chemical Physics.

Supporting Information: Electrostatic interactions contribute to the control of intramolecular thiol-disulfide isomerization in a protein

Denis Maag,[†] Marina Putzu,[†] Claudia L. Gómez-Flores,[†] Frauke Gräter,[‡] Marcus Elstner,[†,¶] and Tomáš Kubař*[,†]

†*Institute of Physical Chemistry, Karlsruhe Institute of Technology (KIT), 76131 Karlsruhe, Germany*

‡*Heidelberg Institute for Theoretical Studies, 69118 Heidelberg, Germany*

¶*Institute of Biological Interfaces (IBG-2), Karlsruhe Institute of Technology (KIT), 76131 Karlsruhe, Germany*

E-mail: tomas.kubar@kit.edu

1 Additional Information and Figures

1.1 Distance vs angle histograms

Based on snapshots taken 10 ps before a transition state is formed, histograms of the S_{nuc}–S_{ctr} distance vs. the S_{nuc}–S_{ctr}–S_{lg} angle were calculated, shown in Fig. S1. The angle bin size is 10° and the distance bin size is 0.2 Å. For a reaction between S32 and S55, when the distance S_{nuc}–S_{ctr} is ca. 2.6 to 3.0 Å, the S–S–S angle lies between 140° and 180°. In reactions between S32 and S55, the angles lie between 120° and 180°.

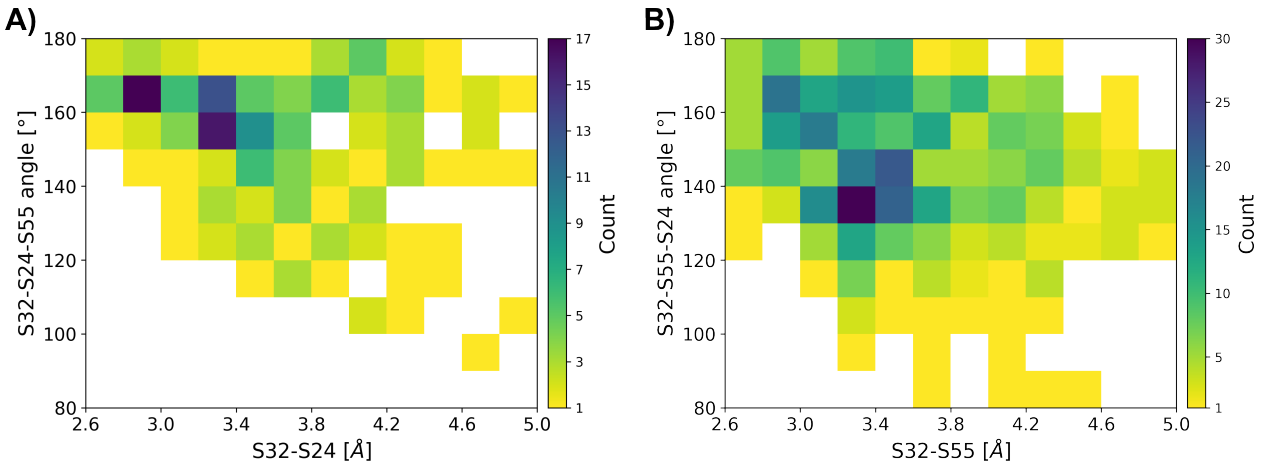

Figure S1: Histograms of the distance and angle distribution based on snapshots 10 ps before a transition state is formed for reactions between S32 and S24 (A), and S32 and S55 (B)

1.2 Example of distances, charges and ESP on the sulfurs before and after a reaction.

Fig. S2 depicts the temporal course of sulfur–sulfur distances, sulfur charges, and ESP on the sulfurs before, during and after a reaction between S32–S24 (left side) and S32–S55 (right side) in two selected simulations. When a transition state is formed, the S_{nuc}–S_{ctr} increases to ca. 2.7 Å and the S_{ctr}–S_{lg} decreases to ca. 2.7 Å, too. The S_{nuc}–S_{lg} distance is slightly smaller than the sum of $|S_{nuc}–S_{ctr}|$ and $|S_{ctr}–S_{lg}|$, thus the angle $S_{nuc}–S_{ctr}–S_{lg} < 180$ °. During the reaction, the negative charge of S32 ($Q(S_{nuc}) \sim -1.1$ e) is transferred to the leaving sulfur S_{lg} ($Q(S_{lg}) \sim -0.1$ e) without any charge accumulation on S_{ctr} ($Q(S_{ctr}) \sim 0$ e). Analogously, the ESP on S_{nuc} and S_{lg} interchange during a reaction whereas the ESP on S_{ctr} does not change much.

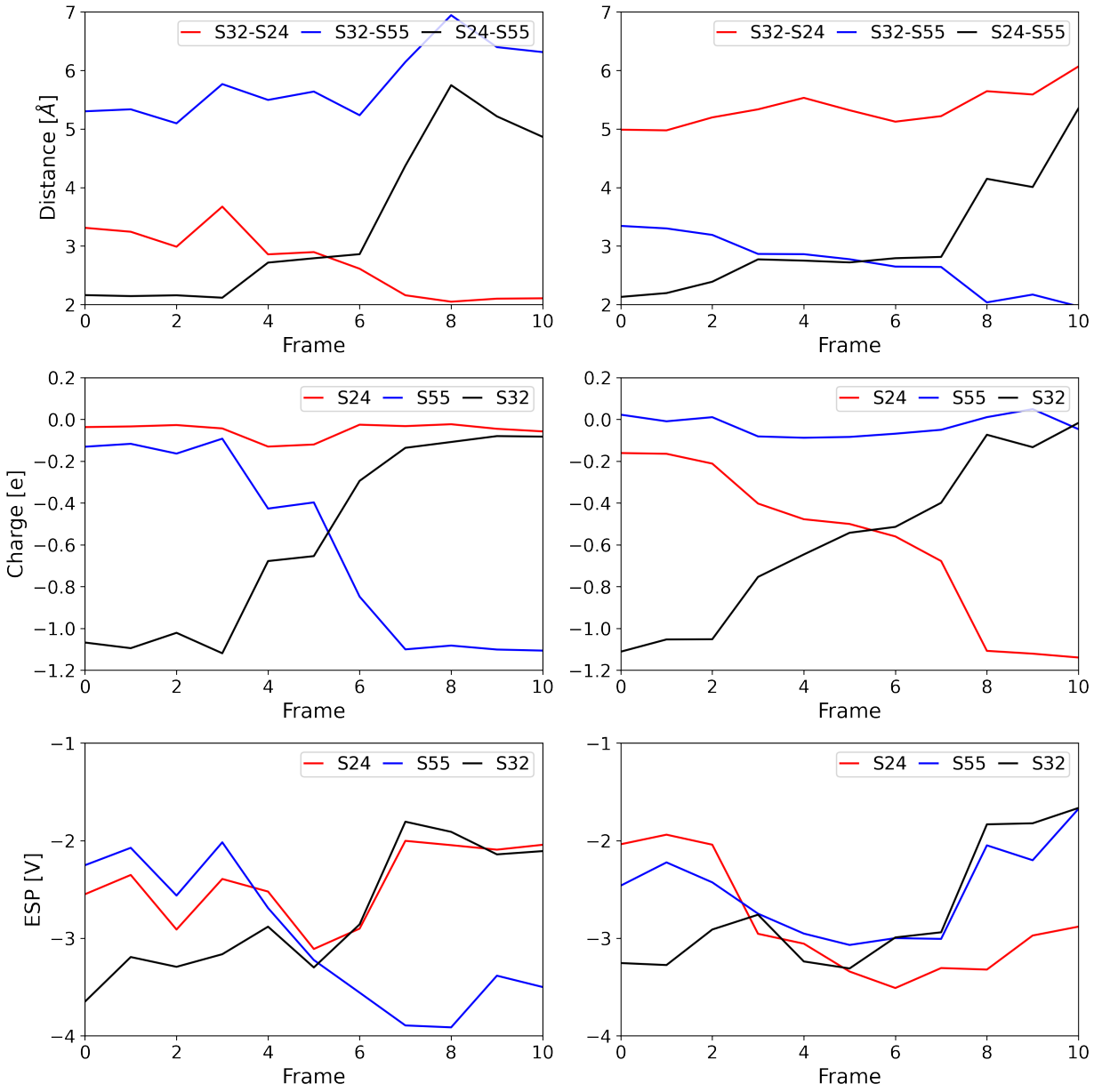

Figure S2: Sulfur–sulfur distances (top), sulfur charges (middle), and ESP on the sulfur atoms (bottom) before, during and after a reaction between S32–S24 (left) and S32–S55 (right) over 11 frames (5.5 ps).

1.3 Contributions to the ESP on the sulfur atoms caused by the MM environment and by the QM atoms.

The electrostatic potential on the sulfur atoms arising from all of the MM atoms is calculated as

$$V_{\mathrm{E}}(\mathbf{r}) = \frac{1}{4\pi\varepsilon_0} \sum_i \frac{q_i}{|\mathbf{r} - \mathbf{r}_i|}$$

(q_i – charge of MM atom i, $\mathbf{r}_i$ – coordinates of MM atom i, $\mathbf{r}$ – coordinates of the atom on which the ESP is calculated).

The ESP caused on a QM sulfur atom by another QM atom corresponds to the DFTB Hamilton shift contribution stemming from the interaction between the atoms,

$$\Phi_a = \Delta q_b \gamma_{ab} + \frac{2}{3} \Delta q_a \Delta q_b \Gamma_{ab} + \frac{1}{3} \Delta q_b^2 \Gamma_{ba}$$

(a – atom on which the ESP is calculated, b – atom which causes the ESP, Δq_a and Δq_b – charges of atoms a and b), where γ_{ab} and Γ_{ab} are analytical functions of interatomic distance; see Ref. 29 for details.

The individual (MM, QM) and combined contributions (QM+MM) are shown in Fig. S3. The ESP arising from the MM atoms is positive with values around 4.5 V (S32), 2.0 V ($\mathrm{S_{ctr}}$), and 1.5 V ($\mathrm{S_{lg}}$). In contrast, the charges of the QM atoms cause a negative contribution to ESP on $\mathrm{S_{ctr}}$ and $\mathrm{S_{lg}}$ of ca. -2.2 V and -1.9 V, respectively. Note that the ESP on $\mathrm{S_{ctr}}$ is now smaller (more negative) than on $\mathrm{S_{lg}}$. The overall ESP is negative, and $\mathrm{ESP(S_{ctr})} < \mathrm{ESP(S_{lg})}$ due to the negative charge of S32 being closer to $\mathrm{S_{ctr}}$.

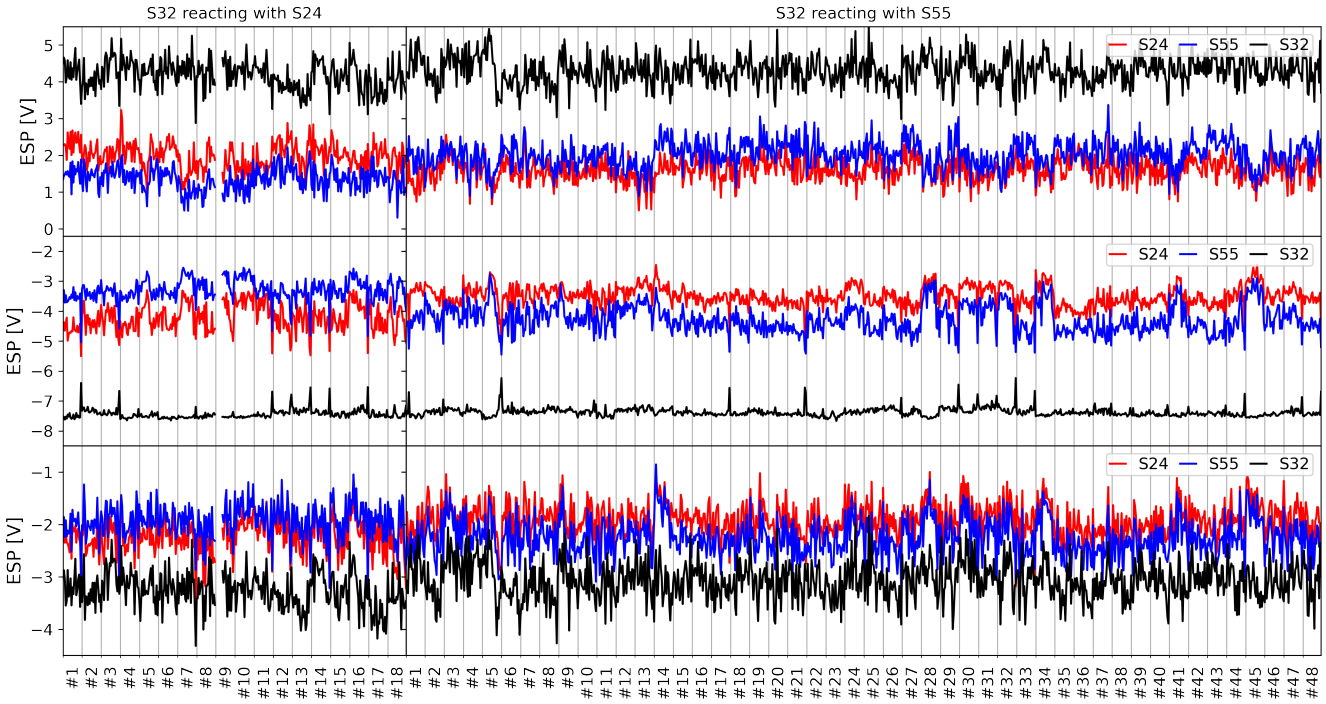

Figure S3: ESP on the three sulfur atoms arising from all MM atoms (top), the QM atoms (middle), and the sum of both (bottom).

1.4 Difference between charges of and ESP on S_{ctr} and S_{lg}

$|Q(S_{lg}) - Q(S_{ctr})|$ and $|ESP(S_{lg}) - ESP(S_{ctr})|$ for both reactions are illustrated in Fig. S4.

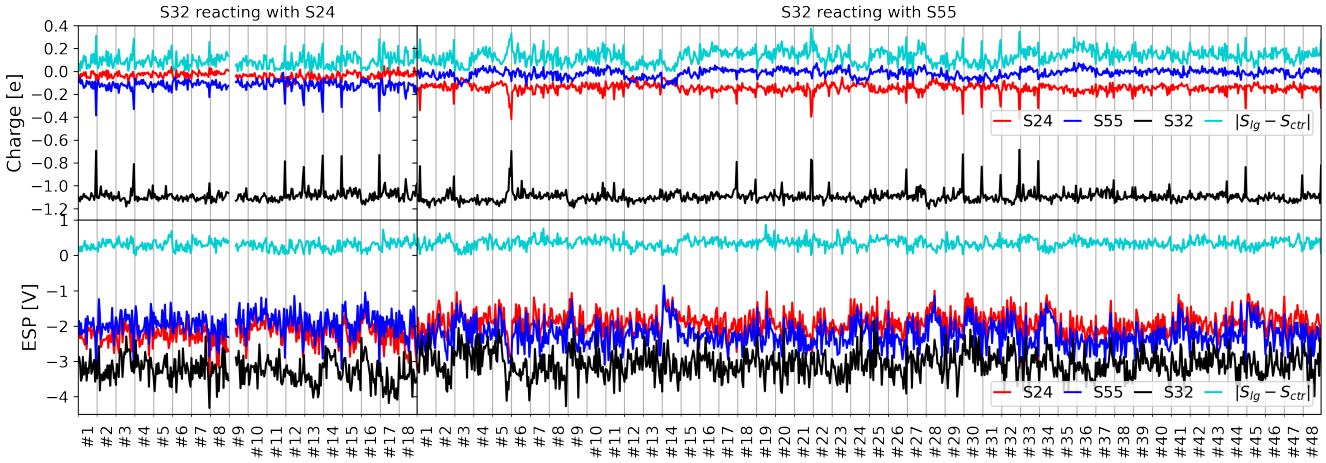

Figure S4: Charges of QM sulfur atoms and the charge difference $|Q(S_{lg}) - Q(S_{ctr})|$ (top). ESP on the QM sulfurs caused by the MM environment and QM atoms, and the ESP difference $|ESP(S_{lg}) - ESP(S_{ctr})|$ (bottom).

1.5 Distance histogram and free energy profile of the distances S32–S24 and S32–S55.

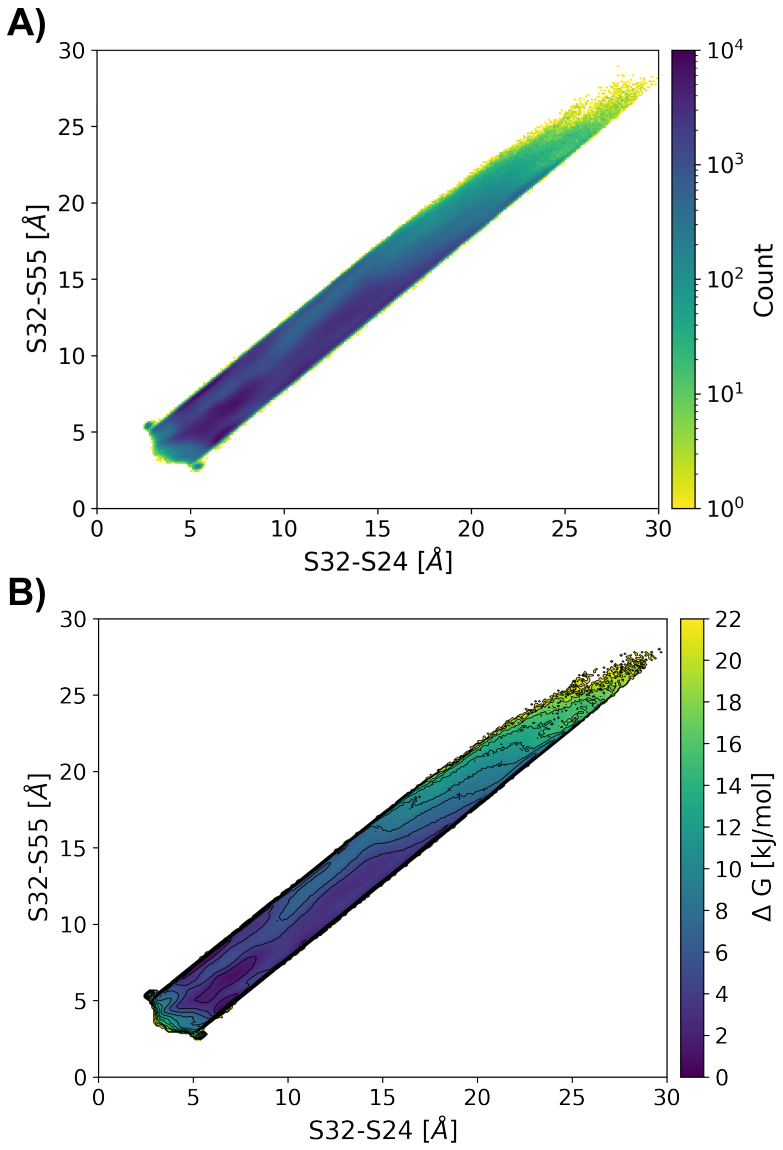

Figure S5: Histogram of distances S32–S24 and S32–S55 (A), converted to a free energy profile (B). Contour lines are drawn every 2 kJ/mol.

1.6 Probabilities of Finding S32 nearer to S24 or S55.

In the "upper" region with 3 Å < |S32–S24| < 10 Å and |S32–S24| < |S32–S55|, S32 was considered to be nearer to S24. In the "lower" region with 3 Å < |S32–S55| < 10 Å and |S32–S24| > |S32–S55|, S32 was considered to be nearer to S55.

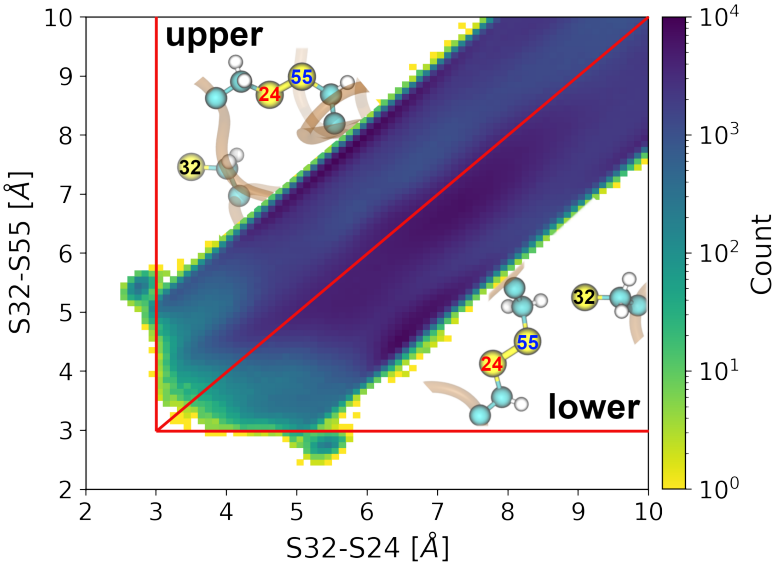

Figure S6: In the upper region, S32 is nearer to S24 and in the lower region nearer to S55.

1.7 Distance histograms and free energy profiles of the S32–S24 and S32–S55 distances for different S24–S55 distances: Potential of the mean force depends on the initial bond length.

To see how the distances between S32 and the disulfide bond correlate with the length of that bond, histograms of the distances S32–S24 and S32–S55 were generated for different S24–S55 bond lengths observed. Specifically, the snapshots collected along the QM/MM simulations were classified into nine different bins with the length of bond S24–S55 ranging from 1.95 to 2.40 Å with a bin width of 0.05 Å. A separate couple of 2D histograms of the distances S32–S24 and S32–S55 were obtained over the snapshots in every bin and were converted to free energy values. Just like above, the probabilities in the "upper" and "lower" regions were summed up, and their ratios were recalculated to free energy differences, which are shown in Fig. S7. Also, all 2D histograms obtained are shown in Figs. S8–S10.

In all bins except the first (1.95–2.00 Å), S32 is closer to S55 on average, and even for large S24–S55 distances, hundreds to thousands occurrences are counted. The energy difference $G_{\text{lower}} - G_{\text{upper}}$ is positive and increases linearly with increasing S24–S55 distance. The maximum distribution of the "upper" region is found at |S24–S55| of 2.05–2.10 Å whereas the maximum of the "lower" region is found at larger bond lengths of 2.10–2.15 Å.

These findings indicate that whenever S32 is closer to S55, a longer S24–S55 bond is favored. Consequently, it may be easier for the system to stretch the bond S24–S55 further to pass to a transition state. By contrast, whenever S32 is closer to S24, a shorter bond is favored and thus a transition state is less likely to form. Still, it should be mentioned that it is difficult to interpret our findings since we are looking for very small energy differences of only a few kJ/mol.

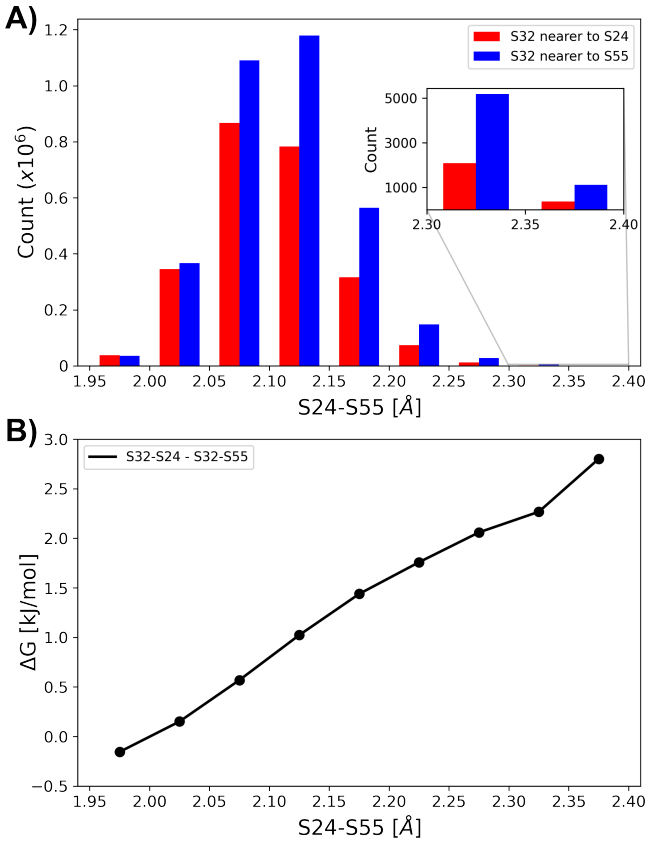

Figure S7: A: Probabilities of finding S32 closer to S24 or S55, depending on the bond length S24–S55. B: The ratio of probabilities in each bin, converted to free energy difference.

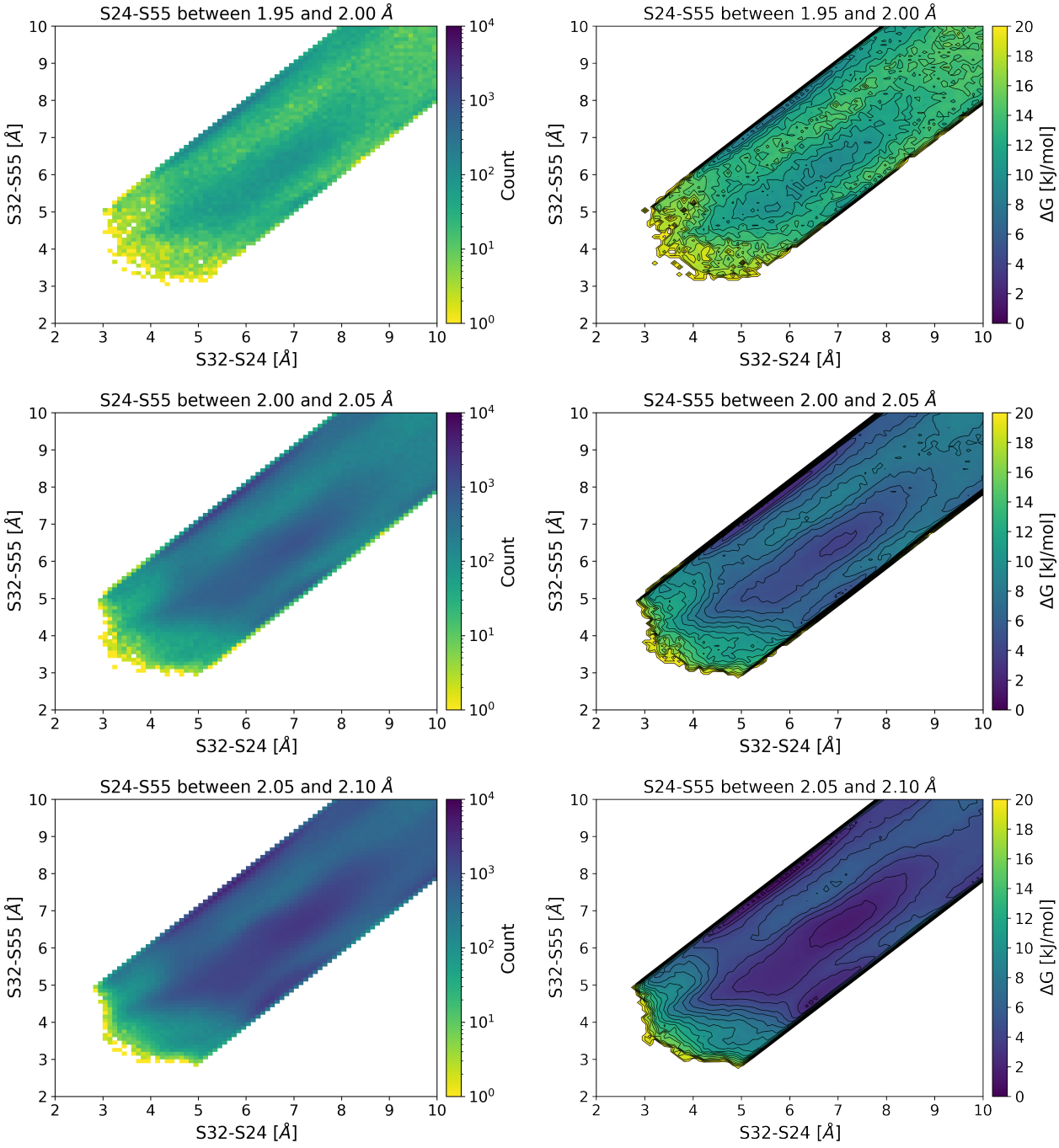

Figure S8: Histograms (left) and the resulting free energy profile (right) of the S32-S24 and S32-S55 distances with S24-S55 distances between 1.95 and 2.00 Å (top), 2.00 and 2.05 Å (middle), 2.05 and 2.10 Å (bottom). Contour lines are drawn every 1 kJ/mol.

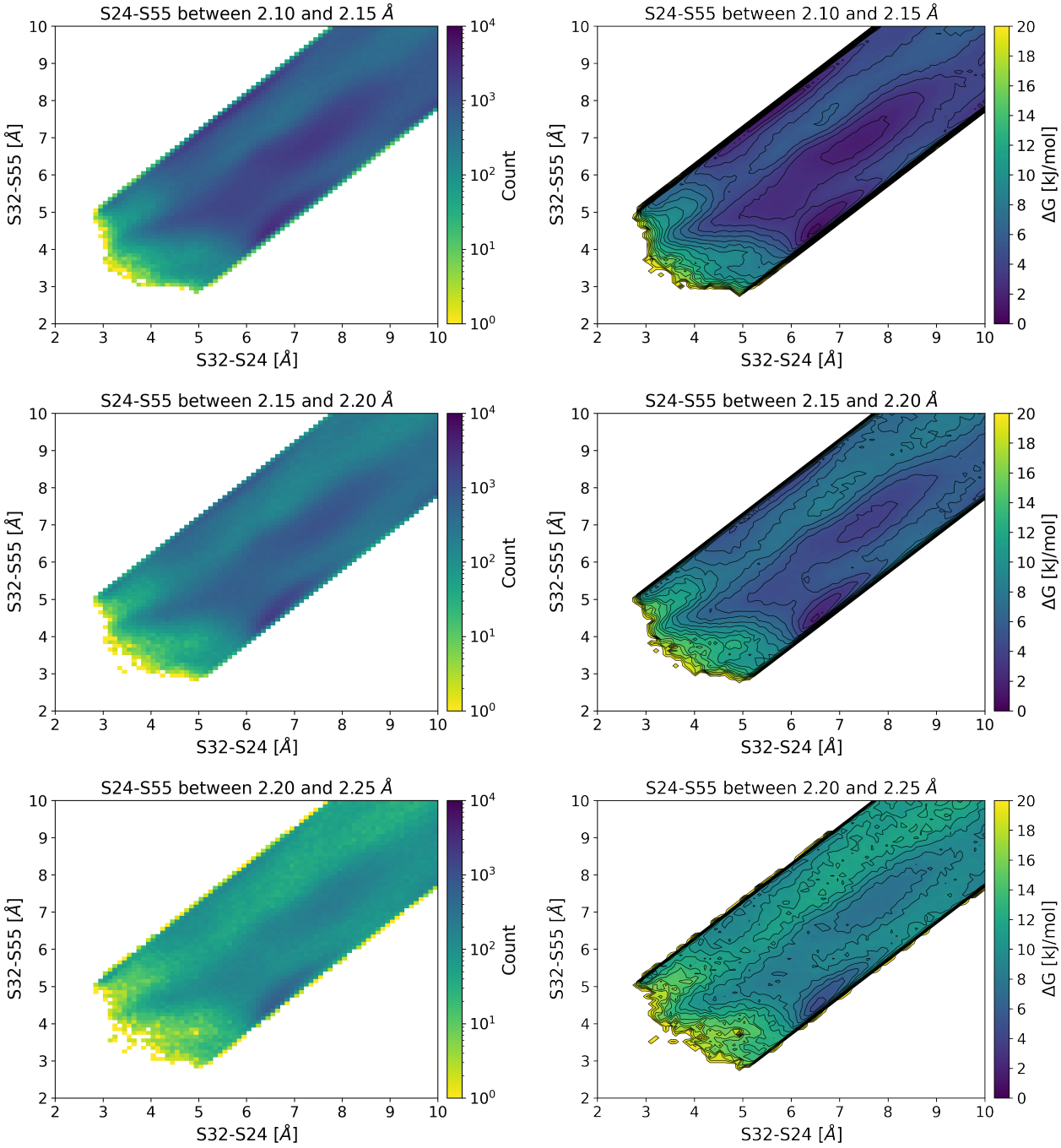

Figure S9: Histograms (left) and the resulting free energy profile (right) of the S32-S24 and S32-S55 distances with S24-S55 distances between 2.10 and 2.15 Å (top), 2.15 and 2.20 Å (middle), 2.20 and 2.25 Å (bottom). Contour lines are drawn every 1 kJ/mol.

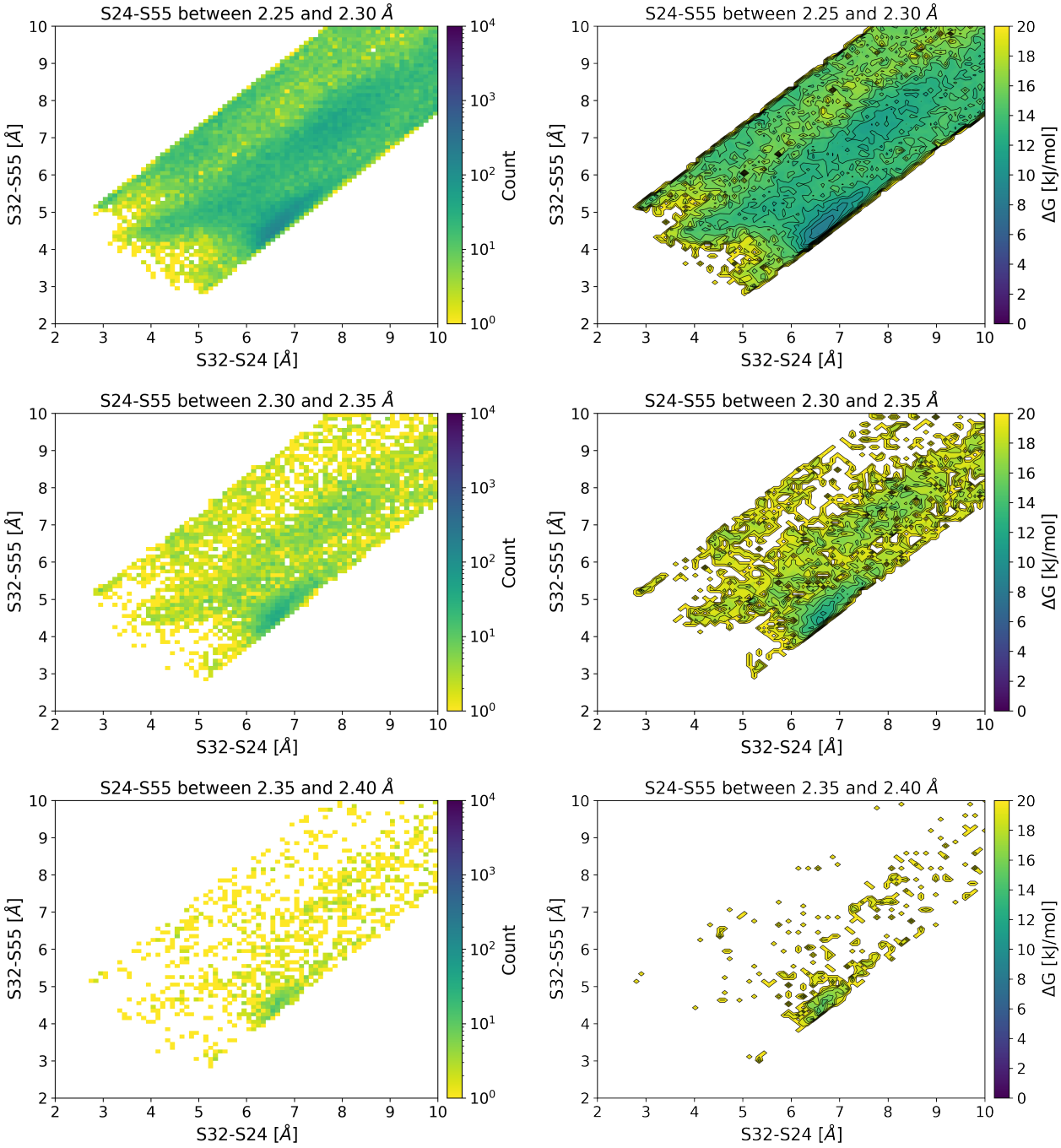

Figure S10: Histograms (left) and the resulting free energy profile (right) of the S32-S24 and S32-S55 distances with S24-S55 distances between 2.25 and 2.30 Å (top), 2.30 and 2.35 Å (middle), 2.35 and 2.40 Å (bottom). Contour lines are drawn every 1 kJ/mol.

1.8 Simulations of the model system

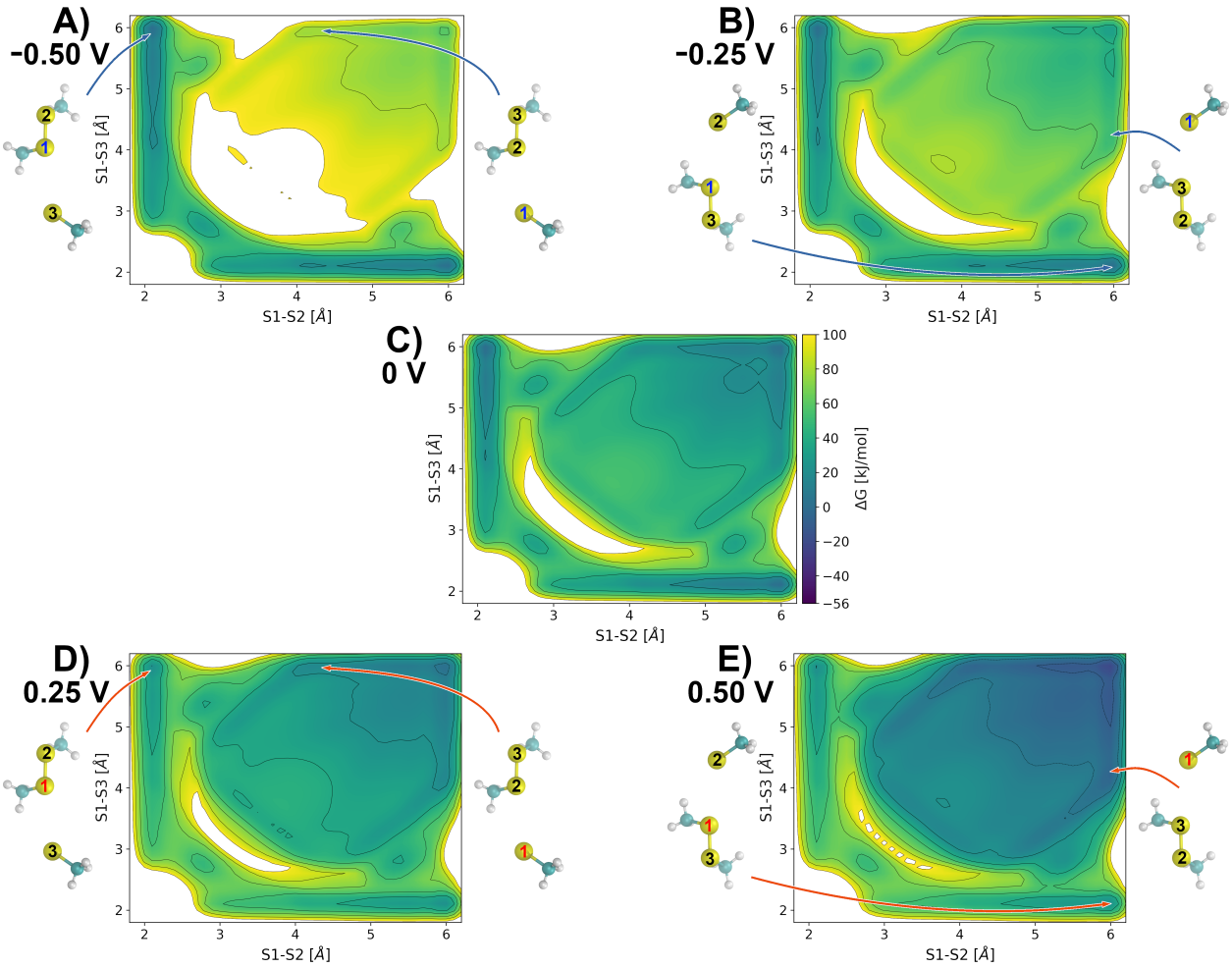

Figure S11: Free energy profiles of the solvated anionic trisulfide system with an additional electric potential imposed onto the atom S_1. Energies of disulfide bonds S_1–S_2 and S_1–S_3 set to zero; contour lines drawn every 20 kJ/mol.

Table S1: Reaction barriers in kJ/mol. *Forward and backward reactions correspond to the same process, so the barriers should be the same.

ESP_{ext} on S_1	reaction	
	S_1–$S_2 \rightleftharpoons S_1$–$S_3$*	S_1–$S_2 \rightleftharpoons S_2$–$S_3$
−0.50 V	47/47	95/36
−0.25 V	50/50	72/40
±0 V	52/52	51/49
+0.25 V	54/54	47/74
+0.50 V	56/56	40/96

2 Metadynamics simulation of disulfide shuffling in I27*

2.1 Methodology

Setup. We performed two well-tempered multiple walker metadynamics simulations to get the free energy profiles of both disulfide exchange reactions, S32 reacting either with S24 (I) or S55 (II). In the multiple walker approach, several separate metadynamics simulations of the same system (walkers) are performed in parallel sharing their deposited biases. The simulations were performed with a local version of Gromacs 2020 patched with Plumed 2.5.1 and interfaced with DFTB+ 19.1. Starting structures for the metadynamics simulations were selected from the 334 QM/MM equilibrated structures matching the following criteria: (a) a reaction occurred in the free QM/MM molecular dynamics simulation with this starting structure; (b) the S_{nuc}–S_{ctr}–S_{lg} angle is greater than 130°. We chose 12 different structures for the S32–S24 reaction setup (I) and 12 different structures for the S32–S55 reaction setup (II). Both metadynamics simulations used 24 walkers, thus the starting structures were duplicated. Each walker was simulated over 2 ns, thus 48 ns in total. A time step of 1 fs (leap-frog integrator) was employed and a temperature of 300 K (Bussi thermostat) and a pressure of 1 bar (Parrinello–Rahman barostat) were maintained. Electrostatic interactions between the QM and MM regions were scaled down by a factor of 0.75. The S_{ctr}–S_{lg} and S_{nuc}–S_{ctr} distances were used as collective variables (CV) to drive the reactions, i.e. (I) S24–S55 and S32–S24, and (II) S24–S55 and S32–S55 Gaussian biasing potentials with an initial height of 1.2 kJ/mol and a width of 0.2 Å were deposited every 1 ps in each walker with a bias factor of 20. The bias exchange period of the walkers was set to 1 ps.

Additional restraints. The configurational space of each reaction was reduced by applying harmonic restraints to S_{ctr}–S_{lg} distances > 3.5 Å and S_{nuc}–S_{ctr} distances > 10 Å with a force constant of $100\,000\,\mathrm{kJ\,mol^{-1}\,nm^{-1}}$. Additionally, the S_{nuc}–S_{ctr}–S_{lg} angle was restrained to values $> 130°$ with a force constant of $100\,000\,\mathrm{kJ\,mol^{-1}\,rad^{-1}}$. Since metadynamics puts biases on both distances, the disulfide bond will elongate over time and eventually break

even without the sulfur anion S_{nuc} having approached close enough for a reaction. To avoid bond breaking while the sulfur anion is too far away, additional restraints were applied to the sum of the three sulfur–sulfur coordination numbers, which were defined as

$$s_S(r_{ij}) = \frac{1 - \left(\frac{r_{ij}}{r_0}\right)^n}{1 - \left(\frac{r_{ij}}{r_0}\right)^m} \tag{1}$$

with the parameters taking values of $r_0 = 2.9$ Å, $n = 10$ and $m = 20$ for all considered combinations; $s_S(r_{S_{32}S_{24}})$, $s_S(r_{S_{32}S_{55}})$ and $s_S(r_{S_{24}S_{55}})$. The parameters where chosen in a way, so that the restraints do not interfere with the transition state. When the sum of all three coordination number was > 1.82, i.e. a disulfide bond length of ca. 2.3 Å without the sulfur anion in proximity, harmonic restraints with a force constant of $20\,000\,\mathrm{kJ\,mol^{-1}\,nm^{-2}}$ were applied to avoid further elongation of the bond.

2.2 Results

Multiple-walker well-tempered QM/MM metadynamics simulations were performed with the intention to resolve the free energy profile of both thiol–disulfide shuffling reactions and to estimate the genuine energy barriers. However, the corresponding free energies do not converge even after a combined simulation time of 48 ns for each reaction, although the biases being added are very small. The energy profiles after a simulation time of 24 ns, 30 ns, 36 ns, 42 ns, and 48 ns are shown in Fig. S12, the height of the barriers are in Fig. S13, and the temporal courses of the respective CV (the S–S distances) are shown in Figs. S14 and S15. The barrier heights for S32→S24 fluctuate between 19–22 kJ/mol, and for S32→S55 between 22–27 kJ/mol. Nevertheless, they are in the same order of magnitude with those obtained from the 334 free QM/MM molecular dynamics, cf. Fig. 2 in the main text. Such a barrier height is also compatible with the many occurrences of the reactions observed on a nanosecond timescale. The location of free energy minima for S32 approaching S24 or S55 also agree with those obtained from the unbiased MD simulations well.

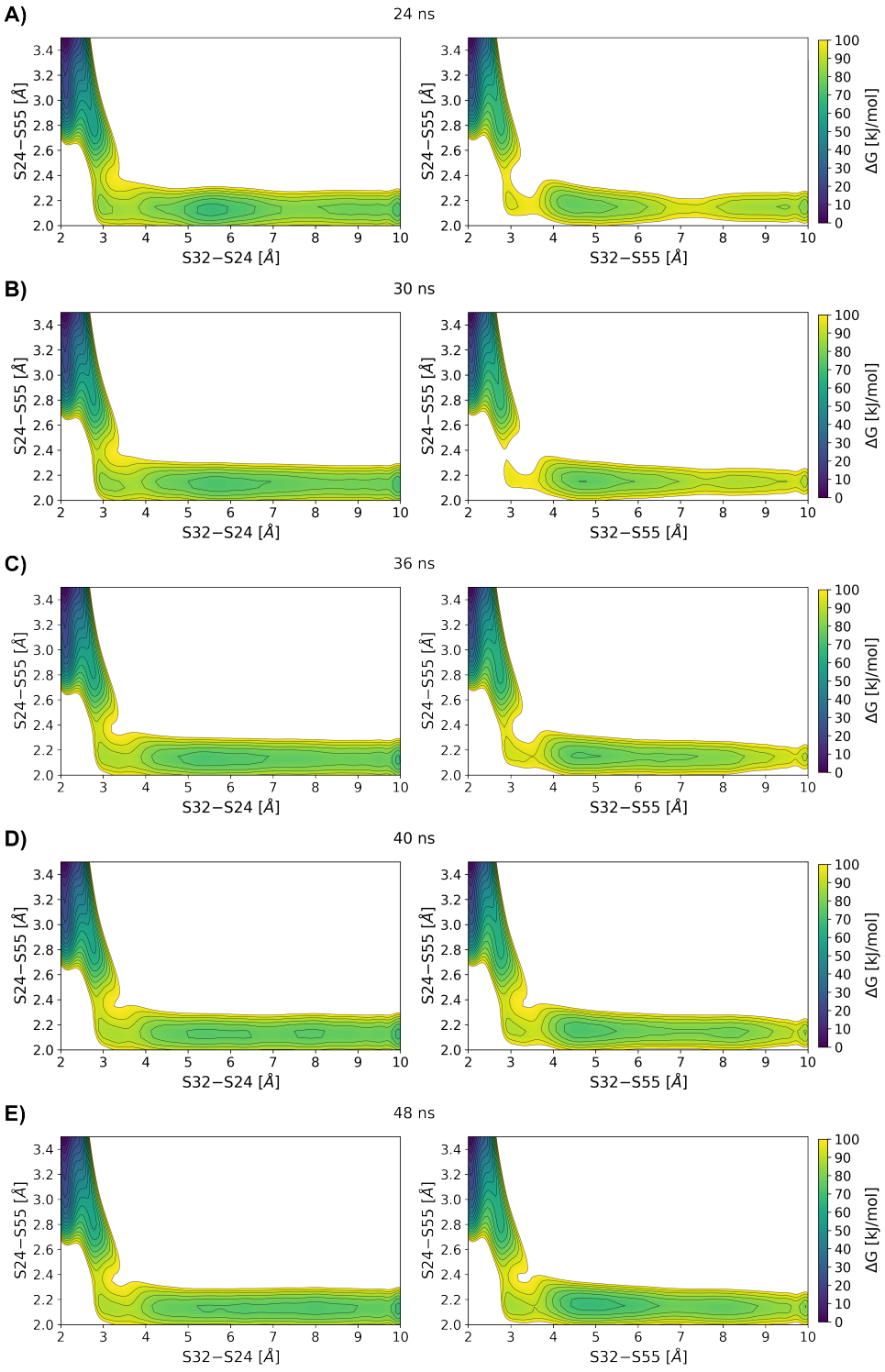

Figure S12: Free energy profiles of the 2D metadynamics simulations of S32 reacting with S24 (left) and S55 (right) after a total simulation time of 24 ns (A), 30 ns (B), 36 ns (C), 40 ns (D), and 48 ns (E).

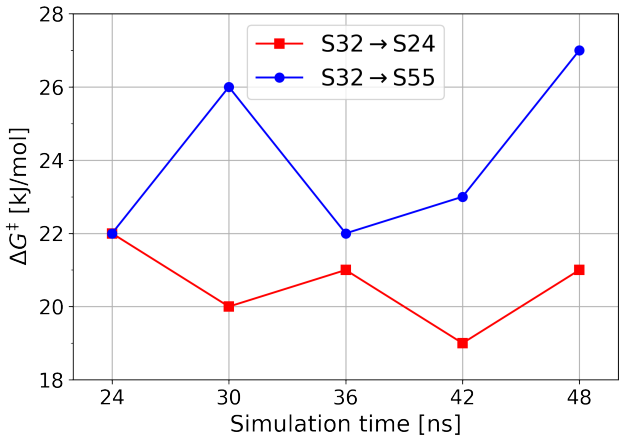

Figure S13: Barrier heights of the 2D metadynamics simulations of S32→S24 and S32→S55 after a total simulation time of 24 ns, 30 ns, 36 ns, 40 ns, and 48 ns.

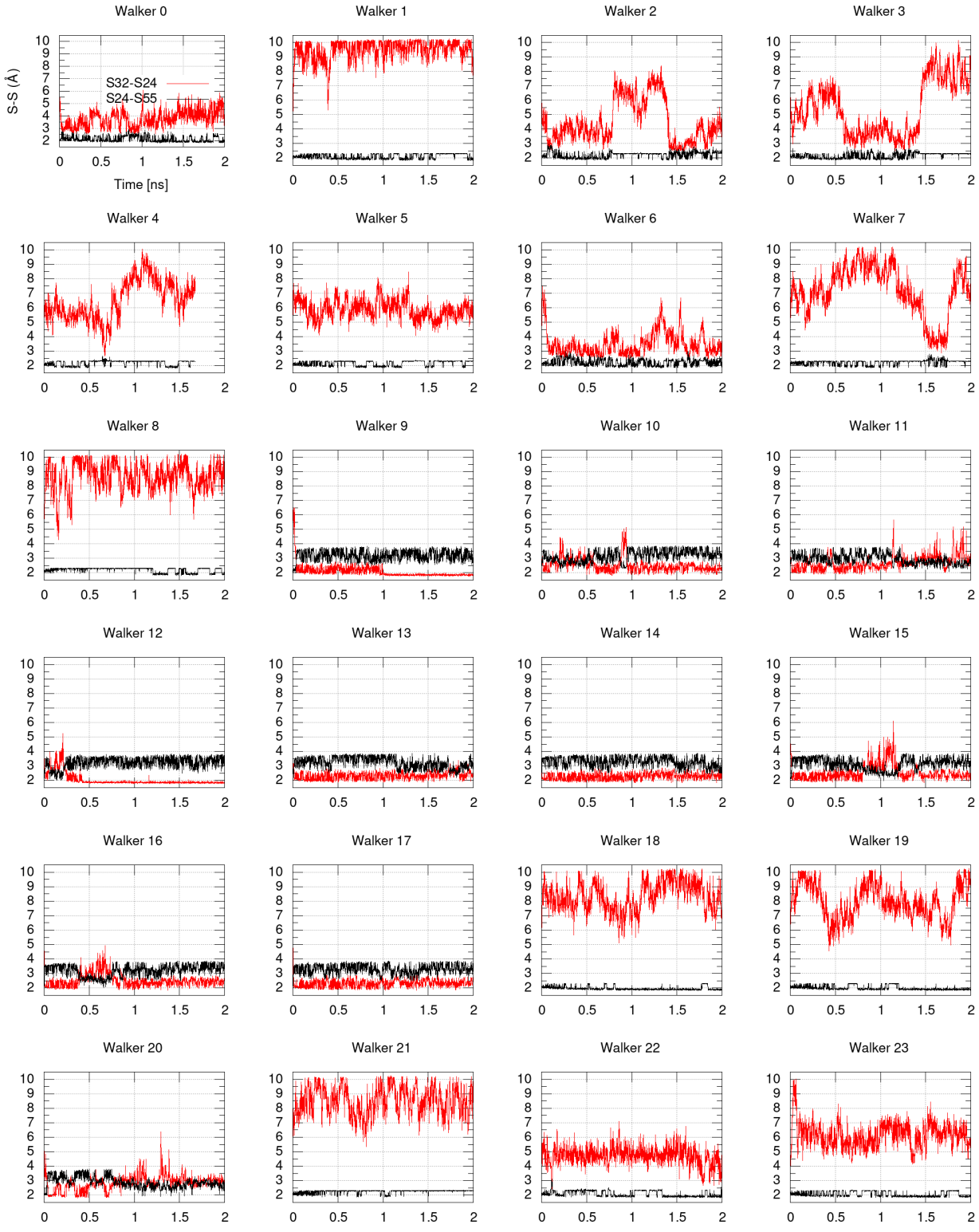

Figure S14: Temporal course of the reaction coordinate values of the S32→S24 multiple-walker metadynamics.

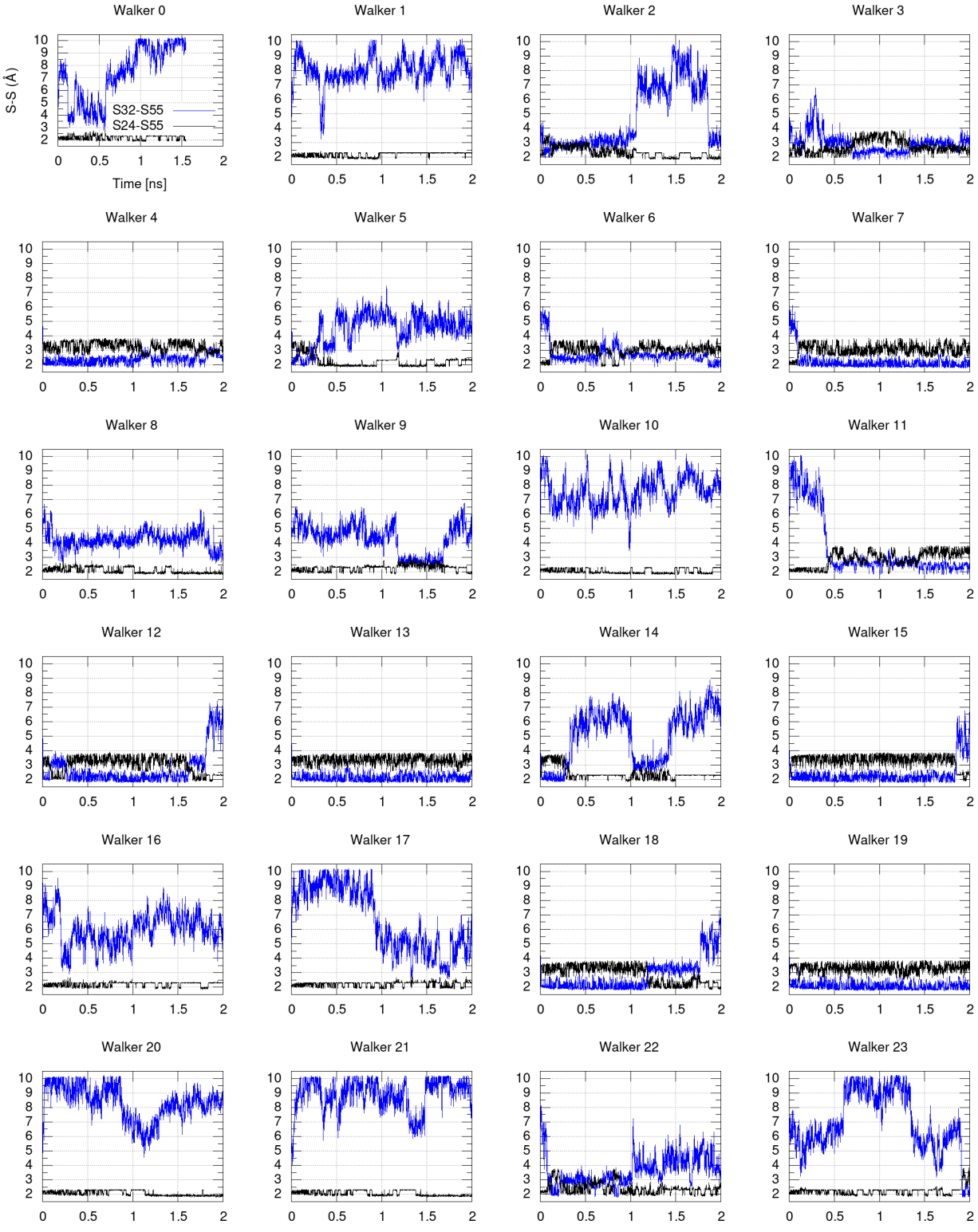

Figure S15: Temporal course of the reaction coordinate values of the S32→S55 multiple-walker metadynamics. Walker 0 crashed after ∼1.5 ns and thus the total simulation time is ∼23.5 ns.

3 Analysis of system setup and simulation setup

3.1 Mutation of the I27* domain

The complete I27* domain consists of 93 amino acids, 21 of which are charged, and carries a net charge of -7 e, see Tab. S2. Under mechanical stretching stress, the protein strand unfolds up to the disulfide bond between S24 and S55, with the end-to-end distance increasing to ca. 230 Å, see Fig. S16. Hence, an extremely large (long) simulation box would be required to enclose the entire protein strand.

To reduce the box size and thus the computational cost, the molecular system was reduced by removing most of the (completely extended) termini – N-terminus up to Ala19 and C-terminus starting at Gly66. This is justified because the contribution of these termini to the electrostatic potential on the disulfide-bonded sulfur atoms (as discussed in the following) is negligible, and so it their influence on the outcome of the intramolecular thiol–disulfide exchange. After the removal of the first 22 N-terminal and the last 24 C-terminal residues, the truncated protein strand exhibits an end-to-end distance of ca. 60 Å, i.e. one third of the original length.

All of the charged residues that are close to the three reactive cysteines Cys24, Cys55 and Cys32 are located on the loop formed by residues 25 to 54 and are therefore retained in the truncated I27* domain. The nearest charged residue in the termini (that are to be truncated) is Glu17, and its distance from the closest reactive Cys24 is at least $6 \times 4 = 24$ Å, and the other charged residues are further than that. The electrostatic interaction over such a long distance in a system immersed in strongly polarizable aqueous environment vanishes nearly completely.

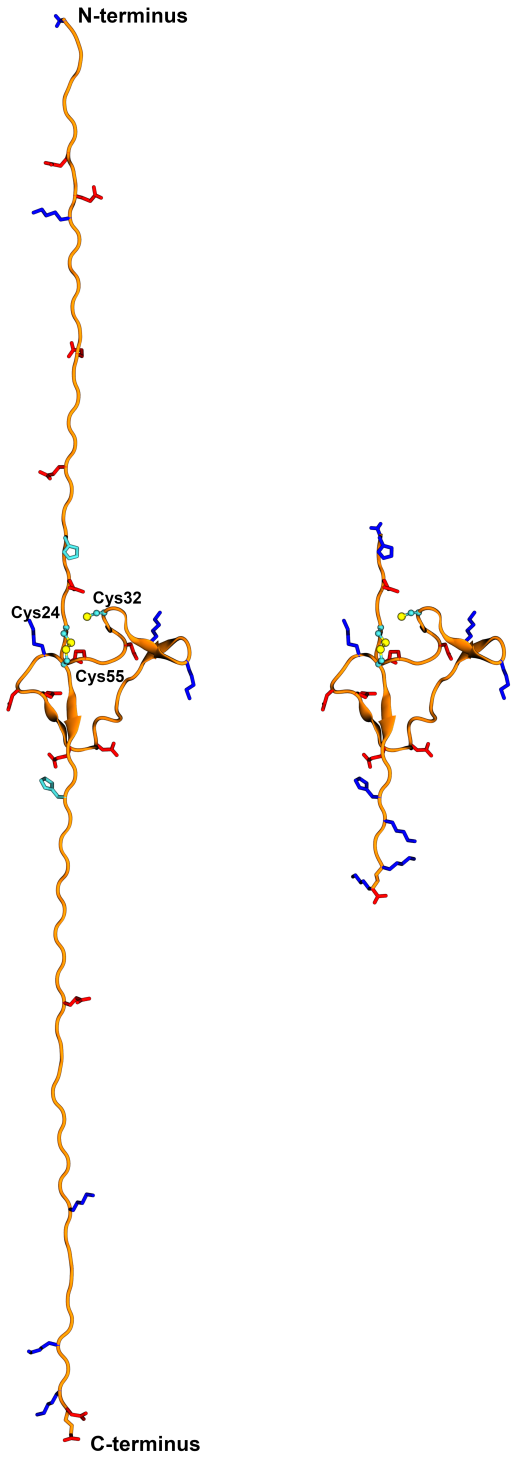

Figure S16: Left: The complete I27* domain after pulling the termini in opposite directions. Right: The truncated I27* domain with mutations introduced at positions 62, 64 and 65. Negatively charged residues – red, positively charged residues – blue, neutral histidines in the full I27* – cyan (these are protonated thus positively charged in the truncated I27*).

The net charge of the truncated I27* domain is -5 e. Five positively charged residues were introduced by means of mutations, in order (i) to reproduce the electrostatic relationships in the complete protein as closely as possible, and additionally (ii) to achieve charge neutrality of the system. (The more common way of electroneutralization by means of adding counterions was tested in pilot simulations, which oftentimes showed instability whenever the counterions approached the reaction center.) None of the mutations are located (i) within 30 Å of Cys24 and Cys55, nor (ii) on the flexible loop between Cys24 and Cys55. In the original I27* domain, the N-terminal segment (residues -3 to 23) carries a net charge of $Q_{\mathrm{N-term}} = -3$ e, and the C-terminal segment (residues 56 to 89) is elcetroneutral, $Q_{\mathrm{C-term}} = 0$ e. The charge difference between the two segments is $\Delta Q = Q_{\mathrm{N-term}} - Q_{\mathrm{C-term}} = -3$ e.

Without any treatment of charges, the truncated I27*, which consists of the residues 20–65 and has both termini ionized, both the N-terminal and C-terminal chains carry one negative charge each, $Q_{\mathrm{N-term}} = Q_{\mathrm{C-term}} = -1$ e, so that $\Delta Q = 0$ e. The original charge difference and charge neutrality are achieved by (i) mutating the remote residues Asn62, Gln64, and Leu65 (located at least $6 \times 4 = 24$ Å away from the nearest reactive Cys55) to lysines, and (ii) protonation of the two histidines His20 and His61, see Fig. S16 and Tab. S2. After these modifications, the truncated I27* domain exhibits $Q_{\mathrm{N-term}} = 0$ e and $Q_{\mathrm{C-term}} = +3$ e, so that the charge difference of $\Delta Q = -3$ e is restored.

Table S2: Amino acid sequence of the full I27* domain and the truncated I27* domain considered in this work. Negatively charged residues – red, positively charged residues – blue, disulfide-bonded cysteines – brown.

#	full	trunc.	#	full	trunc.	#	full	trunc.
			20	HIS	HIS	66	GLY	
			21	PHE	PHE	67	MET	
			22	GLU	GLU	68	THR	
			23	ILE	ILE	69	GLY	
			24	CYS	CYS	70	GLU	
			25	LEU	LEU	71	VAL	
			26	SER	SER	72	SER	
			27	GLU	GLU	73	PHE	
			28	PRO	PRO	74	GLN	
			29	ASP	ASP	75	ALA	
			30	VAL	VAL	76	ALA	
			31	HIS	HIS	77	GLN	
			32	CYS	CYS	78	THR	
			33	GLN	GLN	79	LYS	
			34	TRP	TRP	80	SER	
			35	LYS	LYS	81	ALA	
			36	LEU	LEU	82	ALA	
			37	LYS	LYS	83	ASN	
			38	GLY	GLY	84	LEU	
			39	GLN	GLN	85	LYS	
			40	PRO	PRO	86	VAL	
			41	LEU	LEU	87	LYS	
			42	ALA	ALA	88	GLU	
-3	GLY		43	ALA	ALA	89	LEU	
-2	ALA		44	SER	SER			
-1	MET		45	PRO	PRO			
0	ALA		46	ASP	ASP			
1	LEU		47	CYS	CYS			
2	ILE		48	GLU	GLU			
3	GLU		49	ILE	ILE			
4	VAL		50	ILE	ILE			
5	GLU		51	GLU	GLU			
6	LYS		52	ASP	ASP			
7	PRO		53	GLY	GLY			
8	LEU		54	LYS	LYS			
9	TYR		55	CYS	CYS			
10	GLY		56	HIS	HIS			
11	VAL		57	ILE	ILE			
12	GLU		58	LEU	LEU			
13	VAL		59	ILE	ILE			
14	PHE		60	LEU	LEU			
15	VAL		61	HIS	HIS			
16	GLY		62	ASN	LYS			
17	GLU		63	CYS	CYS			
18	THR		64	GLN	LYS			
19	ALA		65	LEU	LYS			

3.2 Ensemble of starting structures – is there any bias?

The distribution of the S–S distances in the ensemble of starting structures as well as in the ensemble of structures obtained from the QM/MM equilibration simulations are shown in Tab. S3 and Fig. S17. In both ensembles, S32 is not necessarily significantly closer to either S24 or S55; rather, there are structures in which the distances |S32–S24| and |S32–S55| are similar. Furthermore, in most of the structures, S32 is either too far from or not linearly aligned with S24 and S55, so a reasonable S–S–S transition state cannot form quickly. The distribution of S–S distances is even more scattered and shifted to larger distances after the initial QM/MM equilibration phase. Interestingly, the maxima in the histograms already correspond to those in the histogram over all 334 QM/MM MD simulations in Fig. S5, i.e. the minima on the PMF in Fig. 2 in the main text.

In the "start S24" batch (S32 closer to S24 in the starting structure), the reaction S32→S24 occurred 17× while S32→S55 occurred 22× for a total of 39 reactions. In the "start S55" batch (S32 closer to S55 in the starting structure), the reaction S32→S24 occurred only once while S32→S55 occurred 26× for a total of 27 reactions. Hence, there are two important observations: (i) even though "start S24" contains 14 fewer structures than "start S55", more reactions occurred; (ii) preference for S32→S55 is found even in "start S24" where S32 is closer to S55 initially. We can conclude that ratio of the reaction outcome is not influenced (biased) by the unequal numbers of starting structures in the ensembles.

Table S3

	taken from Ref. 13		after QM/MM equil.	
	start S24	start S55	start S24	start S55
$\lvert$S32–S24$\rvert < \lvert$S32–S55$\rvert$	126	0	109	29
$\lvert$S32–S24$\rvert > \lvert$S32–S55$\rvert$	0	152	40	129
$\lvert$S32–S24$\rvert \approx \lvert$S32–S55$\rvert$	34	22	11	16

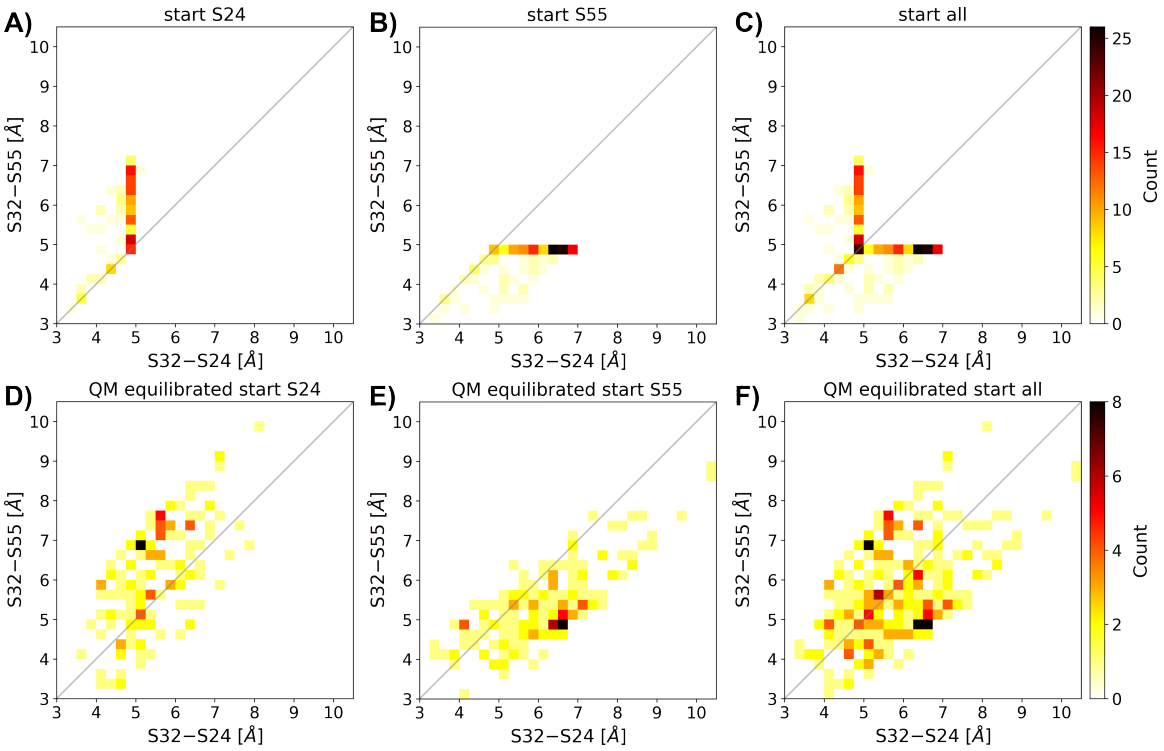

Figure S17: Histograms of the S32–S24 and S32–S55 distances in the ensemble of structures taken from Ref. 13 (A–C) and among the structures yielded by QM/MM equilibrations (D–F). Left: 160 structures where S32 is closer to S24, center: 174 structures where S32 is closer to S55, right: histograms over the whole ensemble of structures. The bin width is 0.25 Å.

3.3 QM/MM topology

Passing the QM–MM boundary between the Cα and Cβ atoms of an amino acid residue and the removal of MM charges on the side chain starting with Cβ results in a small excess charge in the MM region. For the cystine residue CYX in the Amber force field used here, this excess charge of +0.0051 e is very small. In this work, charge neutrality was achieved by redistributing the negative of the excess charge on the atoms Cα and Hα equally, and this charge set was used for Cys24, Cys32 and Cys55. In another, more common approach, the charges of Cα and Hα would be removed altogether in order to prevent overpolarization of the QM region, and the negative of excess charge of −0.1144 would be redistributed on the backbone atoms N and C (or optionally, on N, HN, C and O).[S1] The atomic charge sets are compared in Tab. S4.

Table S4: MM charge sets on the reactive cysteine/cystine residues used in this work. "force field" corresponds to the CYX residue in the Amber force field.

atom	force field	this work	ALT approach
Cα	+0.0429	+0.0403	0
Hα	+0.0766	+0.0741	0
N	−0.4157	−0.4157	−0.3585
H	+0.2719	+0.2719	+0.2719
C	+0.5973	+0.5973	+0.6545
O	−0.5679	−0.5679	−0.5679
sum	+0.0051	0	0

In this section, we compare the approach in the current work with the removal of Cα+Hα and an alternative redistribution of excess charge to N and C ("ALT"). To do so, single-point QM/MM calculations were performed along four short trajectories using a topology with the ALT approach. Two trajectories were taken from each batch, "start S24" and "start S55", such that the reaction S32→S55 occurred in one of them and S32→S24 occurred in the other. Subsequently, the charges of the QM sulfur atoms obtained from these ALT calculations were compared with those from the original QM/MM MD simulations. The temporal course of

the charges are shown in Fig. S18, and the averaged differences of charges obtained with the two approaches are listed in Tab. S5.

Table S5: Difference of charges of sulfur atoms yielded by the approach used in current work and the ALT approach; $\Delta Q = Q_{\text{current}} - Q_{\text{ALT}}$. Mean values and standard deviations given.

Batch and reaction	ΔQ(S24) [e]	ΔQ(S55) [e]	ΔQ(S32) [e]
start S24, S32→S24	+0.01 (0.02)	+0.01 (0.02)	+0.05 (0.02)
start S24, S32→S55	+0.00 (0.02)	+0.01 (0.02)	+0.06 (0.02)
start S55, S32→S24	+0.02 (0.02)	+0.00 (0.02)	+0.05 (0.02)
start S55, S32→S55	+0.00 (0.02)	+0.01 (0.02)	+0.06 (0.02)

Merely the sulfur atom of the Cys32 anion carries a charge that is on average 0.06 more negative with the ALT approach than with the approach applied in the current work. Importantly, there is no significant difference of charges of the sulfur atoms of the nucleophilic target residues Cys24 and Cys55. Therefore, it appears that the exact way to distribute the excess charge among the MM atoms does not largely impact the calculated properties.

References

(S1) König, P. H.; Hoffmann, M.; Frauenheim, T.; Cui, Q. A Critical Evaluation of Different QM/MM Frontier Treatments with SCC-DFTB as the QM Method. *J. Phys. Chem. B* **2005**, *109*, 9082–9095.

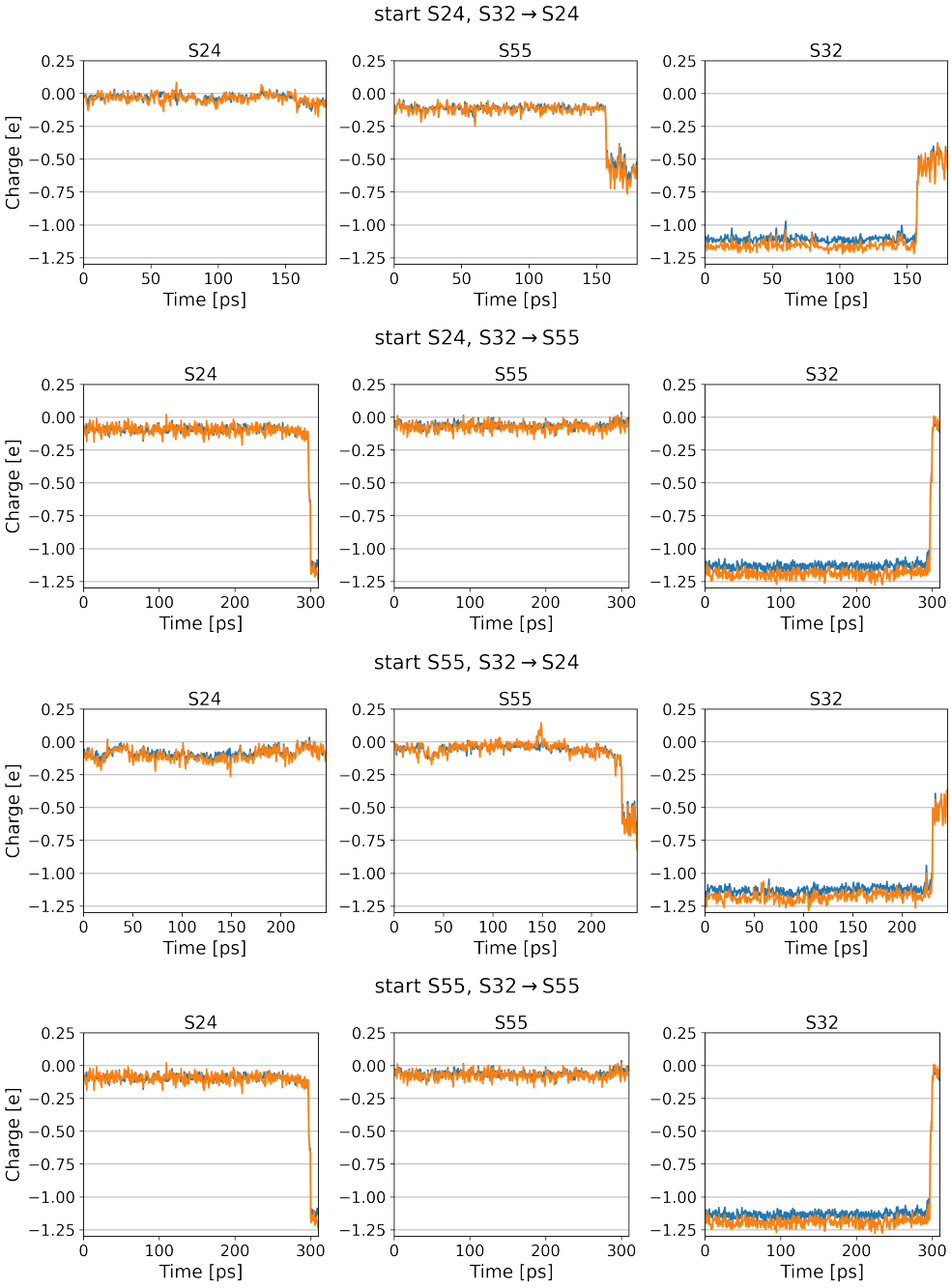

Figure S18: Temporal course of charges of sulfur atoms; blue – MM charges used in this work, orange – ALT MM charges. Selected was one trajectory from each batch with each reaction outcome.